Research Article

Molecular Docking Study, Synthesis and Evaluation of Antitumor Activity of Novel Pyrazole Derivatives

J. Nelson Samuel Jebastin[1]*, T. Ramesh Kumar[1] and D. Evangelin[2]

[1]Department of Zoology, Annamalai University, Annamalai Nagar-608 002, Tamil Nadu, India.
[2]Department of Information Technology, Sri Vidya Engineering College, Virudhunagar, Tamil Nadu, India.

ABSTRACT
Cancer therapies targeted developing cell cycle-based mechanism that emulates the body's natural process in order to stop the growth of cancer cells. This approach can limit the damage to normal cells and the accompanying side effects caused by conventional chemotherapeutic agents. Inhibition of histone deacetylase (HDAC) enzymes is emerging as an innovative and effective approach for the treatment of cancer. Sixteen compounds of pyrazole derivatives were designed and tested in silico for their interaction with histone deacetylase (HDAC8) enzyme. 16 ligands docked with Histone deacetylase 8 Human HDAC8 (PDB ID: 1T69) using GLIDE program (Version 5.0, Schrodinger, LLC, New York, 2008) and designed, synthesized and evaluated for their ability to inhibit cell proliferation in cancer cell lines. Based on the docking score 4-(5-Bromo-2-hydroxybenzylideneamino)-1,5-dimethyl-2-phenyl-1H-pyrazol-3(2H)-one showed highest docking score of -6.4061, which is important for HDAC8 inhibition. In this present investigation, molecular docking, design, synthesize and evaluated for *in vitro* antitumor activity to identify novel active compound targeting the HDAC8 protein. Among the 16 compounds A13 showed promising activity against human cervical cancer cell line.

Keywords: *In vitro* anticancer, Histone deacetylase 8, synthesis, Molecular Docking.

INTRODUCTION

HDAC has been classified into three classes. Class 1 and 2 classified on the basis of sequence similarity Class 1 includes HDAC 1-3 and 8, which are homologus to yeast RPD3 found in nucleoplasm, Class 2 includes HDAC 4-7, 9-10, which are homologus to yeast Hda1 found in nucleus and cytoplasm and Class 3 includes HDAC11. Class 1 and 2 operated by zinc dependent and class 3 by NAD mechanism[1-5]. HDACs are involved in cell-cycle progression and differentiation, and their deregulation is associated with several cancers[6].

HDAC inhibitors interact with chromosomes in the cancer cell and causes cancer cells to stop growing. The first HDAC drug approved by U.S Food and Drug Administration is SAHA (suberoylanilide hydroxamic acid or vorinostat) for treating Cutaneous T-cell Lymphoma[7]. SAHA inhibits the activity of class I & II HDACs[8]. Mutations or alterations that induce loss of function of class I HDACs may contribute to cancer development[9]. The tumor-suppressor gene RB requires the recruitment of class I HDACs to repress gene transcription Thus, the loss of class I HDAC activity could induce the expression of genes regulated by Rb, thereby suppressing their protective role in tumour development. The present investigation involves molecular docking studies of virtually designed pyrazole derivatives and the synthesis and evaluation of *in vitro* anti tumour activity potential HDAC8 inhibitors.

MATERIALS AND METHODS

Computational Design to choose best novel heterocyclic compound derivatives based on target based drug discovery

Total 16 compounds are designed virtually based on the QSAR and pharmacophore model)[10] as 2-Phenyl-1,2-dihydro-3H-pyrazol-3-one (Figure 1). Pyrazole derivative is optimized using aromatic and acceptor groups and the ligands are listed in Table 1. The ligands are sketched using ISIS Draw and

these are given as input to prepare ligand module in Glide. This generates 3D structures, tautomers, isomers and filters the ligands by Lipinski rule of five. After applying the force fields on ligands the structures are minimized for lowest energy.

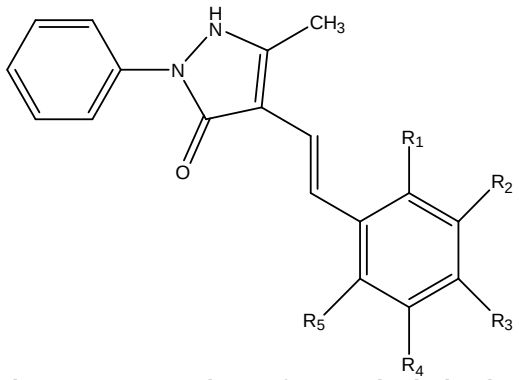

Fig. 1: Parent nucleus of Pyrazole derivative

Table 1: Pyrazole derivatives (A1-A16)

Compound	R1	R2	R3	R4	R5
A1	H	CH_3	H	H	OH
A2	H	OH	H	H	OH
A3	H	OH	CH_3	H	OH
A4	H	OH	OH	H	OH
A5	H	OH	OH	CH_3	OH
A6	H	H	H	H	OH
A7	H	OH	OH	OH	OH
A8	H	Cl	H	OH	OH
A9	H	Cl	H	OH	OH
A10	H	Cl	H	H	OH
A11	H	Cl	H	H	NH2
A12	H	Cl	NH_2	H	NH2
A13	**H**	**Br**	**H**	**H**	**OH**
A14	NH_2	Cl	NH_2	H	NH_2
A15	NH_2	Cl	$NHNH_2$	H	NH_2
A16	NH_2	Br	$N(NH_2)_2$	H	NH_2

Docking Methodology

The steps involved in docking are as follows:

Ligand structure

The chemical structure of each ligand was drawn using build module**.**

Ligand preparation

In order to prepare high quality, all-atom 3D structures for large numbers of drug-like molecules, starting with the 3D structures in SD Maestro format, LigPrep was used. LigPrep produced a single, low energy and 3D structure for each successfully processed input structure.

Preparation of protein: Molecular docking were performed for 16 compounds using the GLIDE program (Version 5.0, Schrodinger, LLC, New York, 2008) to understand the interaction of 3k with HDAC8. The Maestro user interface (version8.5, Schrodinger, LLC, New York, 2008) was employed to set up and execute the docking protocol and also for analysis of the docking results. Human HDAC8 (PDB ID: 1T69) was selected for docking studies and was prepared for docking through protein preparation wizard, energy minimization has been carried out using OPLS2001 force field. Maestro and prepared for docking through Ligprep module (energy minimized using MMFF force field). GLIDE grid generation wizard has been used to define the docking space. Docking was performed using SP (Standard Precision mode) docking protocol.

Receptor Grid Generation: Receptor grid generation requires a “prepared” structure: an all atom structure with appropriate bond orders and formal charges. Glide searches for favourable interactions between one or more ligand molecules and a receptor molecule, usually a protein. The shape and properties of the receptor are represented on a grid by several different sets of fields that provide progressively more accurate scoring of the ligand poses. The options in each tab of the Receptor Grid

Generation panel allow defining the receptor structure by excluding any co-crystallized ligand that may be present, determine the position and size of the active site as it will be represented by receptor grids, and set up Glide constraints. A grid area was generated around the binding site of the receptor.
Ligand Docking: This is carried out using Glide Dock. Glide searches for favourable interactions between one or more ligand molecules and a receptor molecule, usually a protein. Each ligand acts as single molecule, while the receptor may include more than one molecule, e.g., a protein and a cofactor. Glide was run in rigid or flexible docking modes; the latter automatically generated conformations for each input ligand. The combination of position and orientation of a ligand relative to the receptor, along with its conformation in flexible docking, is referred to as a ligand pose. The ligand poses that Glide generates pass through a series of hierarchical filters that evaluate the ligand's interaction with the receptor. The initial filters test the spatial fit of the ligand to the defined active site, and examine the complementarity of ligand-receptor interactions using a grid-based method patterned after the empirical ChemScore function. Poses that passed these initial screens entered the final stage of the algorithm, which involves evaluation and minimization of a grid approximation to the OPLS-AA non bonded ligand-receptor interaction energy. Final scoring is then carried out on the energy-minimized poses.

Glide Extra-Precision Mode (XP)
The extra-precision (XP) mode of Glide combines a powerful sampling protocol with the use of a custom scoring function designed to identify ligand poses that would be expected to have unfavourable energies, based on a well-known principles of physical chemistry. The presumption is that only active compounds will have available poses that avoid these penalties and also receive favourable scores for appropriate hydrophobic contact between the protein and the ligand, hydrogen-bonding interactions, and so on. The chief purposes of the XP method are to weed out false positives and to provide a better correlation between good poses and good scores. Extra-precision mode is a refinement tool designed for use only on good ligand poses. Finally, the minimized poses are re-scored using Schrödinger's proprietary GlideScore scoring function. GlideScore is based on ChemScore, but includes a steric-clash term and adds buried polar terms devised by Schrodinger to penalize electrostatic mismatches: Glide Score = 0.065*vdW + 0.130*Coul + Lipo + Hbond + Metal + BuryP + RotB + Site.
QikProp[11] is a quick, accurate, easy-to-use absorption, distribution, metabolism, and excretion (ADME) prediction program designed by Professor William L. Jorgensen. QikProp predicts physically significant descriptors and pharmaceutically relevant properties of organic molecules, either individually or in batches. In addition to predicting molecular properties, QikProp provides ranges for comparing a particular molecule's properties with those of 95% of known drugs. QikProp also flags 30 types of reactive functional groups that may cause false positives in high-throughput screening (HTS) assay.

Synthesis
Synthesis of 4-(5-Bromo-2-hydroxybenzylideneamino)-1,5-dimethyl-2-phenyl-1H-pyrazol-3(2H)-one
Exactly 2.009g (10mmol) of 5-Bromosalicylaldehyde was dissolved in 50ml of methanol and taken in a 150ml beaker. Exactly 2.03g (10 mmol) of 4-Aminoantipyrine was dissolved separately in 50ml of methanol. The methanolic solution of 5-Bromosalicylaldehyde was stirred vigorously at room temperature using a magnetic stirrer. Then the methanolic solution of 4-Aminoantipyrine was added in drops to the above solution with constant stirring for a period of 20 minutes. Yellow precipitate was formed after the complete addition of the amine solution. To ensure the completion of the reaction, the reaction mixture was further stirred for another 6 hrs at room temperature. After 6h of stirring at room temperature, the reaction mixture was refluxed at 60^0 C for half an hour with constant stirring. Then the reaction mixture was cooled to room temperature. The yellow precipitate formed during the course of the reaction was filtered, washed several times with cold methanol and dried over calcium chloride in a desiccator.

Characterization
FTIR Analysis
IR spectra of all Schiff bases and their metal complexes were obtained in Perkin Elmer FTIR spectrometer using Potassium Bromide pellets in the range of 400-4000cm^{-1}.

NMR Studies

^{1}H-NMR experiments for all the Schiff bases synthesized were performed in a Bruker 500 MHz NMR instrument. About 2-3mg of ligands was dissolved in 0.5ml of $CDCl_3$ in a NMR tube. About 50 scans were performed for every spectrum. In all the cases Tetramethylsilane (TMS) was used as an internal standard. All the spectra obtained were corrected with respect to TMS. The software Mestrec 2.0 was used to evaluate the peak positions and their integrations.

^{13}C-NMR experiments for all the Schiff bases synthesized were performed in a Bruker 125 MHz NMR instrument. About 30-40mg of ligands was dissolved in 0.5ml of either DMSO-d_6 or $CDCl_3$ in a NMR tube. About 1000 scans were performed for all the experiments. All the spectra obtained were corrected with respect to the solvent signal.

UV-VIS Spectroscopy

The UV-Vis spectra for all the Schiff bases and their metal complexes were obtained in 10^{-3} M solution of Ethanol at room temperature using Perkin Elmer UV-Vis-NIR spectrometer. Glass cuvettes were used for the measurements in the UV-Vis region. The baseline was corrected with respect to Ethanol in all the case. For all experiments the spectral range was scanned from 200-800nm. The scan rate was kept constant (100 nm/sec) for all the experiments.

Fluorescence Spectroscopy

The fluorescence spectra for all the Schiff bases and their metal complexes were performed in a10^{-6} M solution of Ethanol at room temperature using a Perkin Elmer LS-55 spectrofluorometer. Quartz fluorescence cell were used for the measurements in the solution state. The excitation and emission slit width was maintained at 5.0nm for all the experiments. The sample was either excited at 270nm or at 380nm. The fluorescence spectra were recorded over the range 200-800nm. A slow scan rate was maintained for all the experiments.

In Vitro Anti Cancer Activity[12]

The human cervical cancer cell line (HeLa) was obtained from National Centre for Cell Science (NCCS), Pune, and grown in Eagles Minimum Essential Medium containing 10% fetal bovine serum (FBS).

For screening experiment, the cells were seeded into 96-well plates at plating density of 10,000 cells/well and incubated to allow for cell attachment at 37^0C, 5% CO_2, 95% air and 100% relative humidity[13-15]. After 24h the cells were treated with serial concentrations of the samples. The samples were initially dissolved in dimethylsulphoxide (DMSO) and further diluted in serum free medium to produce five concentrations. One hundred microliters per well of each concentration was added to plates to obtain final concentrations of 100, 10, 1, 0.1 µM. The final volume in each well was 200µl and the plates were incubated at 37^0C, 5% CO_2, 95% air and 100% relative humidity for 48h. The medium containing without samples were served as control. Triplicate was maintained for all concentrations[16-17].

After 48h of incubation, 15µl of MTT (5mg/ml) in phosphate buffered saline (PBS) was added to each well and incubated at 37^0C for 4h. The medium with MTT was then flicked off and the formed Formosan crystals were solubilized in 100µl of DMSO and then measured the absorbance at 570nm using micro plate reader. The % cell inhibition was determined using the following formula[18].

% cell Inhibition = 100- Abs (sample)/Abs (control) x100

Nonlinear regression graph was plotted between % Cell inhibition and Log_{10} concentration and IC_{50} was determined using Graph Pad Prism software

RESULTS AND DISCUSSION

All the 16 ligands were docked in the active site of Human HDAC8 (PDB ID: 1T69) using Glide Dock. Compounds were ranked based on the docking score. The docking score of all ligands are presented in Table 2. Heterocyclic functional group of all the molecules were found to be close to Zn^{2+} atom in the active site, and establishes a hydrogen bond with (A13) ASP331, which shows the major and favourable interaction of the ligands with HDAC8 .Amongst the 16 molecules docked, compound A13 was the one with the best Glide and E model score of (-40.88) (Figure 2). It exhibited one hydrogen bonding interaction with active site amino acids.

Table 2: Components of Glide Score of Docking (Extra-Precision Mode)

Code	XP GScore	glide e model	glide energy	XP HBond	glide pose no.
A13	-6.4061	-40.8825	-29.7795	-0.69	13

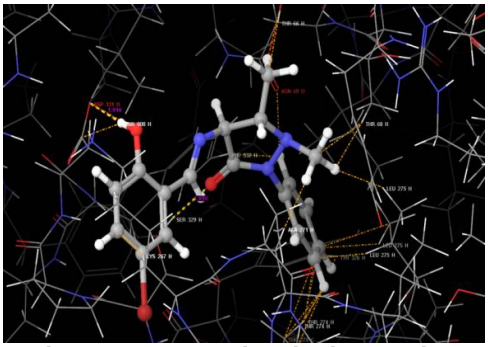

Fig. 2: HDAC8 molecular interaction with compound A13

Synthesis

A Schiff base is a class of compound derived by the condensation of aldehydes or ketones with amines. Schiff base compounds contain a carbon-nitrogen double bond with the nitrogen atom connected to an alkyl or aryl group. (Scheme 1)

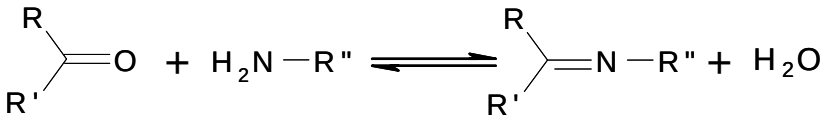

Scheme. 1: The General Schiff base condensation reaction Synthesis of A13

The synthetic route for compound A13 shown in scheme 2. The methanolic solution of 5-Bromosalicylaldehyde was stirred with the methanolic solution of 4-Aminoantipyrine vigorously at room temperature produced 4-(5-Bromo-2-hydroxybenzylideneamino)-1,5-dimethyl-2-phenyl-1H-pyrazol-3(2H)-one as yellow solid in 87.2% (3.365g) yield.

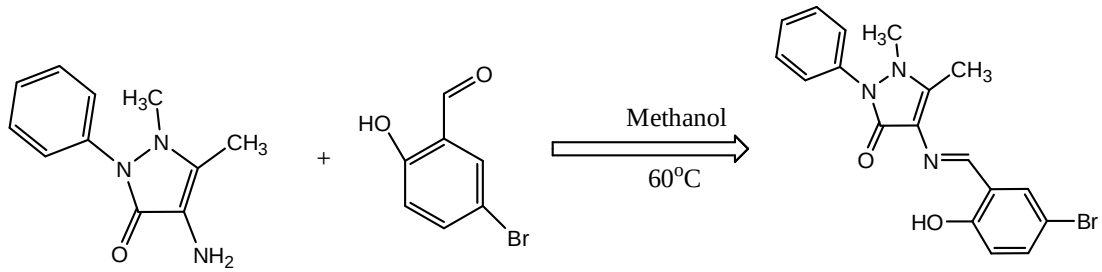

Scheme. 2: Synthesis of 4-(5-Bromo-2-hydroxybenzylideneamino)-1,5-dimethyl-2-phenyl-1H-pyrazol-3(2H)-one.

UV-VIS Spectrum

The electronic spectrum of the compound A13 is recorded in10^{-6} M solution of Ethanol at room temperature. Two broad bands at 254 and 363nm are observed in the UV-Vis spectra of Figure 3(a). The band at the 254 nm is attributed to the benzene π-π* transition. Another band at 363nm is due to

n- π* transition of the non-bonding electrons presents on the nitrogen of the azomethine group in Schiff base.

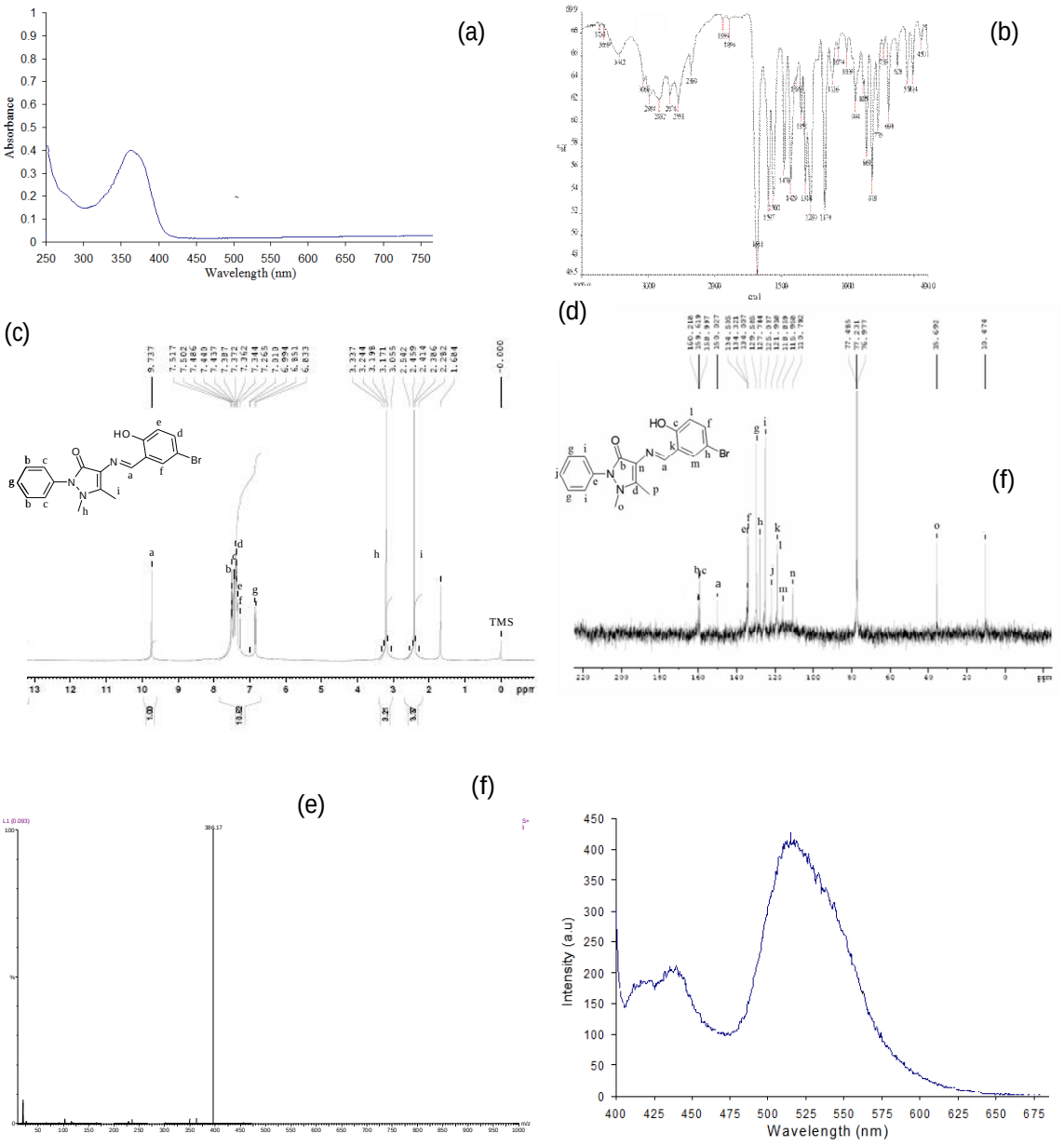

Fig. 3: Spectral studies of compound A13 (a): UV-VIS spectra of ligand A13 in ethanol at 25°C; (b): FTIR spectrum of Schiff base; (c): ^{1}H-NMR spectra in $CDCl_3$; (d): ^{13}C-NMR (^{1}H decoupled) spectra in $CDCl_3$; (e): Mass Spectrum; (f): Fluorescence spectra in ethanol at 25°C (λ_{ex} = 380nm)

IR spectrum

The IR spectrum of Schiff base compound A13 is given in Figure 3 (b). The characteristic band at 1597cm^{-1} corresponds to the presence of –C=N group in the molecule which in turn suggest the formation of Schiff base. A strong and intense band is also observed in 1681cm^{-1} corresponds to the –C=O stretching frequency of antipyrine unit in the molecule. The Schiff base also showed a broad

intense band peak 3442cm^{-1}, a characteristic feature for –OH stretching frequency indicating the existence of free –OH group in the Schiff base.

^{1}H-NMR studies

The ^{1}H NMR Spectra of ligand compound A13 is shown in the Figure 3(c). The spectra of ligand compound A13 consists of 5 sets of non-equivalent proton. The signal at δ=9.7ppm is due to the proton of azomethine group (CH=N-). The signal at δ=7.51-6.28 is due to protons of the benzene ring. The signal at δ=3.3 is due to three protons of the N-CH_3 group. The signal at δ=2.41 is due to three protons of methyl group (-CH_3). It appears at up field. It supports the overall structure of the product and conform the product formation.

^{13}C-NMR Studies

The ^{13}C-NMR spectra of compound A13 is shown in Figure 3(d). The spectram of Compound A13 Consists of many sets of nonequivalent carbon atoms. The Peak observed at 160 and 159ppm is due to Cabonyl carbon and C-O carbon pf phenyl ring. This carbon atom is highly deshielded, because it is a part of the Carbonyl group and hence the Signal appears at downfield. The peak at 150ppm is due to azomethine carbon. The regions from 120-140ppm are assigned to aromatic carbon, which has high intense signals. But the quaternary carbon shows the lower intensity signal. Methyl carbon appears at upfield region. The two peaks of this upfield region indicate the presence of two methyl group.

Mass Spectra

The mass spectrum of compound A13 recorded in Ethanol and depicted in Figure 3(e). It indicating a intense molecular ion peak at δ386.17 correspond to respective $(M+H)^{+}$ molecular formulae, confirms the formation of Compound A13.

Fluorescence spectrum

The fluorescence emission spectrum of Compound A13 is recorded in 10^{-6} M solution of ethanol at room temperature. Figure 3(f) depicts the fluorescence emission spectra of Compound A13. Two emission bands were observed in the region of 400-450nm and 475-600nm on excitation at 380nm.

In Vitro Anti Cancer Activity

The anti tumour activity of compounds against human cervical cancer cell line (SiHa) was determined by MTT assay method. The human cervical cancer cell line (SiHa) was obtained from National Centre for Cell Science (NCCS), Pune, and grown in Eagles Minimum Essential Medium containing 10% fetal bovine serum (FBS). Cell line was incubated with different concentration for compound A13 and was used to create concentration in various percentage of cell inhibition. These response parameter (IC_{50}) was calculated for each cell line. The synthesized pyrazole derivative compounds were screened against screened (HeLa) human cervical cancer cell line at different concentration are shown in Table 3 and Figure 4.The IC_{50}value corresponds to the compound concentration causing a net 50% loss of initial cells at cell of the incubation period. Compound A13 was found to be more potent and it shows the IC_{50} value at 5.78µM. The standard drug 5-fluro uracil IC_{50} value at 2.836µM revealing that the potency of compound A13 was closer to that of the standard drug IC_{50} value. The higher anticancer potency of compound A13 is probably due to the presence of pyrazole moiety. This might be the reason for the notable difference in IC_{50} values of the synthesized heterocyclic derivatives.

Table 3: The synthesized pyrazole derivative compounds were screened against screened (HeLa) human cervical cancer cell line at different concentration

Code	Cell line	Concentration (µM)	% cell inhibition
Compound A13	HeLa	0.01	3.627968
		0.1	12.26913
		1	32.38786
		10	54.8153
STD (5-Fluoro uracil)	HeLa	0.1	6.675567
		1	30.70761
		10	71.49533
		100	99.3992

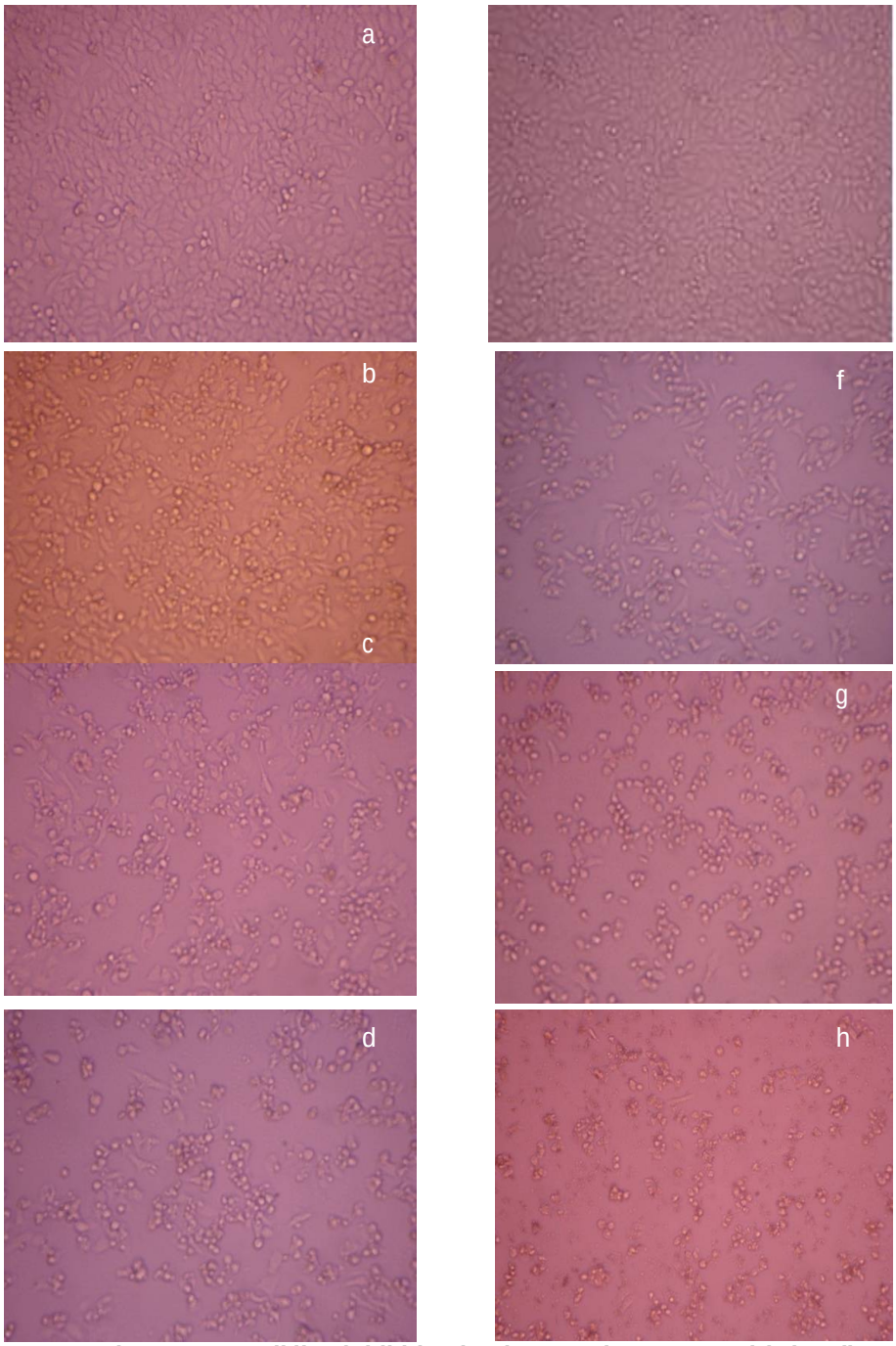

Fig. 4: HeLa cell line inhibition by the sample compound (a,b,c,d) and standard drug (5-fluoro uracil) (e,f,g,h) at 0.1, 1 10 and 100 µM

REFERENCES

1. Ivan VG, Yun Mi L and Holly VG. Molecular Evolution of the Histone Deacetylase Family: Functional Implications of Phylogenetic Analysis. J Mol Biol. 2004;338:17–31.
2. Yang X and Seto E. The Rpd3/Hda1 family of lysine deacetylases:from bacteria and yeast to mice and men. Nat Rev Mol Cell Biol. 2008; 9: 206-218.
3. Bieliauskas AV and Pflum MK. Isoform-selective histone deacetylase inhibitors. Chem Soc Rev. 2008;37:1402–1413.

4. John MD. The Sir2 family of protein deacetylases. Curr Opin Chem Biol. 2005;9:431–440.
5. Yang XJ and Grégoire S. Class II Histone Deacetylases: from Sequence to Function, Regulation, and Clinical Implication. Mol Cell Biol. 2005; 25: 2873–2884.
6. Kouzarides T. Histone acetylases and deacetylases in cell proliferation. Curr Opin Genet Dev. 1999;9:40-8.
7. Walkinshaw DR and Yang XJ. Histone deacetylase inhibitors as novel anticancer therapeutics. Curr Oncol. 2008;15:237-43.
8. Marks PA. Discovery and development of SAHA as an anticancer agent. Oncogene. 2007; 26:1351–56.
9. Glozak MA and Seto E. Histone deacetylases and cancer. *Oncogene.* 2007;26(37):5420-5432.
10. Naresh K, Geetha Ramakrishnan V and Sarma Jagarlapudi S. QSAR Studies of N-(2-Aminophenyl)- Benzamide derivatives as Histone deacetylase2 Inhibitors. Int J PharmTech Res. 2012;4:1110-1121.
11. Ioakimidis L, Loizos T, Amin M, Saira N and Johannes R. Benchmarking the reliability of QikProp. Correlation between experimental and predicted values. QSAR & Combinatorial Science. 2008;27(4):445-456.
12. Wang W, Yuqing Z, Elizabeth RR, Donald LH, Hui W and Ruiwen Z. *In vitro* anti-cancer activity and structure–activity relationships of natural products isolated from fruits of Panax ginseng. Cancer chemotherapy and pharmacology. 2007;59(5):589-601.
13. Boyd MR and Paull KD. Some practical considerations and applications of the National Cancer Institute *in vitro* anticancer drug discovery screen. Drug Dev Res. 1995;34:91-109.
14. Tamm I, Yan Wang ED, Sausville DA. Scudiero NV, Tilman O and John CR. IAP-family protein survivin inhibits caspase activity and apoptosis induced by Fas (CD95), Bax, caspases, and anticancer drugs. Cancer Res. 1998;58(23):5315-5320.
15. Johnson JI, Decker S, Zaharevitz D, Rubinstein LV, Venditti JM and Schepartz S. Relationships between drug activity in NCI preclinical *in vitro* and *in vivo* models and early clinical trials. British journal of cancer. 2001;84(10):1424.
16. Shoemaker M, Bobbi Hamilton SH. Dairkee IC and Michael JC. *In vitro* anticancer activity of twelve Chinese medicinal herbs. Phytotherapy Res. 2005;19(7):649-651.
17. Kelter G, Nigel JS, Katja S, Heinz Herbert F and Matthias T. *In-vitro* anti-tumor activity studies of bridged and unbridged benzyl-substituted titanocenes. Anti-Cancer Drugs. 2005;16(10): 1091-1098.
18. Seeram NP, Lynn SA, Susanne MH, Yantao N, Yanjun Z and Muraleedharan GN. *In vitro* antiproliferative, apoptotic and antioxidant activities of punicalagin, ellagic acid and a total pomegranate tannin extract are enhanced in combination with other polyphenols as found in pomegranate juice. The Journal of nutritional biochemistry. 2005;16(6):360-367.